LIMITED HEIGHTS OF VERTICAL CLIFFS AND MOUNTAIN WALLS LINKED TO FRACTURING IN DEEP TUNNELS - Q-SLOPE APPLICATION IF JOINTED SLOPES

Data de aceite: 02/05/2024

Nick Barton
Nick Barton & Associates, Oslo, Norway

Baotang Shen
CSIRO Energy, Brisbane, Australia

Neil Bar
Gecko Geotechnics Pty, Mt. Sheridan, QLD, Australia

ABSTRACT: Intact brittle rock can fail in tension even when all principal stresses are compressive. This is due to lateral expansion and extension strain when near to a free surface, caused by Poisson's ratio. Exceeding tensile strength due to stress anisotropy and Poisson's ratio are the fracture-initiating conditions around deep tunnels, not the increasing mobilization of compressive strength, commonly beyond 0.4 x UCS. In a related discovery, the limiting height of vertical cliffs and near-vertical mountain walls can also be explained using extension strain theory. The range of limiting heights of approximately 20m for cliffs in porous tuff to record 1,300m high mountain walls in granite are thereby explained. Tensile strength is the weakest link behind cliffs and ultra-steep mountain walls. Sheeting joints can also be explained by extension strain theory. Maximum shear strength is the weakest link when stress levels are ultra-high, or when there is jointing and maximum slope angles is the issue. Here one can use Q-slope. The world's highest mountains are limited to 8 to 9km. This is due to non-linear critical state rock mechanics. It is not due to UCS.

KEYWORDS: Deep tunnels, Cliffs, Mountains; Extension strain; Tensile strength; Shear strength

INTRODUCTION

The lessons from fracturing in deep tunnels is the starting point for the ultra-simple cliff-height and mountain wall-height equation which is introduced in this article. The observed and recently modelled fracturing behavior of deep tunnels in massive rock indicates that fracturing may be initiated by extensional strain over-coming the tensile limit, even when all stresses are compressive. This is possible due to the lateral expansion caused by Poisson's ratio. A small-scale example of this is the acoustic emission

that occurs due to micro-fracture initiation when testing intact rock cylinders in traditional uniaxial compression, where Poisson's ratio is also at work. The commonly used parameter obtained from such tests is σ_c, the unconfined compression strength (commonly written as UCS). This might be 150MPa for granite but only 1.5MPa for weak porous tuff, the medium once used by Christian cliff-dwellers in Cappadocia, Turkey. The tuffs are so weak that there have been many historic cliff failures, which expose old dwellings and Christian churches at irregular intervals. The most basic strength parameter σ_c has traditionally been compared with the estimated maximum tangential ('arching') stress, to investigate if a deep tunnel will suffer fracturing or rock-burst and need more support like sprayed concrete and rock bolts. A newly excavated tunnel results in a big contrast between the maximum tangential ('arching') stress (σ_θ) and the almost unloaded radial stress (σ_r). For elastic isotropic materials and a circular tunnel, the theoretical maximum tangential stress is three times the major principal stress (σ_1) minus the minimum principal stress (σ_2) acting in the same plane, at right angles to the tunnel. At 1,000m depth we might have $\sigma_\theta = 3 \times 30 - 15 = 75$MPa, due to assumed *in situ* stresses σ_v (vertical) and σ_h (horizontal) of 30 and 15 MPa. If we now compare the magnitude of σ_θ with the available uniaxial strength σ_c, say 150MPa for granite, then the ratio $\sigma_\theta/\sigma_c = 75/150 = 0.5$, will suggest from Figure 1 (and from Table 1) that fracturing and break-out may occur: i.e. more support is needed due to much increased SRF i.e. lower Q.

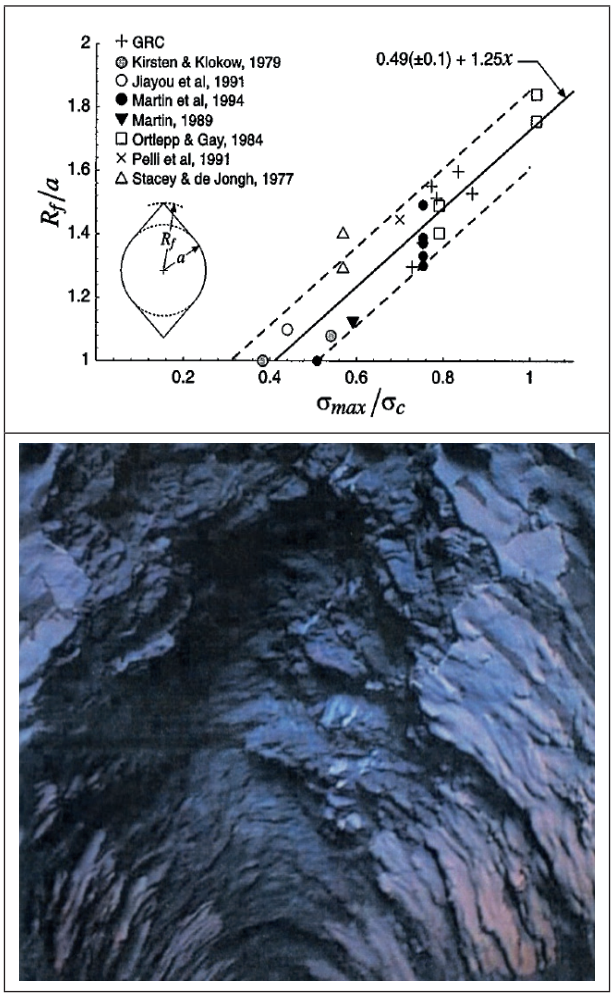

Figure 1. The traditional assumption is that fracturing in a deep tunnel is limited if compressive strength is sufficient. Martin et al. 1998, and Grimstad and Barton, 1993 have independently confirmed that when the stress/strength ratio $\sigma_\theta/\sigma_c \geq 0.4 \pm 0.1$, fracturing and break-out is likely, as illustrated here, to a depth of 2 to 3m. This ocurred in several large diversion tunnels in Brazil (Ita HEP, Barton and Infanti, 2004).

In the Q-system ratings for the stress reduction factor SRF, the rating is accelerated when passing a ratio σ_θ/σ_c of 0.4, as shown in Table 1. The numerous case records collected by Grimstad for the case of deep road tunnels in Norway, giving stress/strength ratios in the case of tunnels of up to 1.4km depth, are given in our illustrated Q-manual (Barton and Grimstad, 2014). Accelerated (i.e. increased) SRF values in the case of high stress give lower Q-values, and therefore the necessary heavier support (closer B c/c, thicker Sfr).

b) Competent rock, rock stress problems		σ_c/σ_1	σ_θ/σ_c	SRF
H	Low stress, near surface, open joints.	> 200	< 0.01	2.5
J	Medium stress, favourable stress condition.	200-10	0.01-0.3	1
K	High stress, very tight structure. Usually favourable to stability, may be unfavourable for wall stability.	10-5	0.3-0.4	0.5-2
L	Moderate slabbing after > 1 hour in **massive** rock.	5-3	0.5-0.65	5-50
M	Slabbing and rock burst after a few minutes in **massive** rock.	3-2	0.65-1	50-200
N	Heavy rock burst (strain-burst) and immediate dynamic deformations in **massive** rock.	< 2	> 1	200-400

Table 1. The 'accelerated' SRF value used in the Q-system S(fr) update of Grimstad and Barton, 1993 when the estimated ratio of σ_θ/σ_c reaches and exceeds 0.4.

The common (but independently suggested) assumption by Grimstad and Barton, 1993 and by Martin et al. 1998 that $\sigma_\theta/\sigma_c \geq 0.4$ will result in 'stress-induced' fracturing, and the need for heavier tunnel support has recently been revisited. Research by co-author Shen using the fracture mechanics code FRACOD (*Shen et a*l. 2013) shows that the assumed 'high stress' fracturing is actually *initiated* by extensional strain, causing the *weakest link* (tensile strength σ_t) to be exceeded first. Propagation by shearing may follow immediately if stress levels (or depth) are sufficient. Shearing may dominate at high stress or when a tunnel (or mine opening) is very deep, and even cause rock bursts, as propagation of fracturing in shear is unstable. (Shen and Barton, 2018). Figure 2 illustrates modes of fracturing seen or modelled in simulations of deep tunnels. Numerical modelling with the displacement discontinuity (DDM) based FRACOD code is also shown. This was a study specifically to see the effect of jointing on reducing the risk of rock-burst, due to dissipation of shear and tensile stresses with the help of the jointing. In deep rock tunnels, the presence of significant jointing appears to reduce the risk of fracturing and rock bursts, while in shallow tunnels, the presence of jointing, and of course faulting, increases the risk of collapse, if insufficient tunnel support is applied. The FRACOD models shown in Figure 2 show 1,000m deep simulations with $\sigma_{1\ (horizontal)} = 2\ \sigma_{2\ (vertical)}$. The effect of jointing is to partly dissipate the fracturing of intact rock. (See numerous examples in Shen and Barton, 2018). Red fractures are tensile, green are shear, with respectively mode I and mode II fracture toughness. In the top of Figure 2 we see a physical model of intersecting log-spiral shear fracturing caused by boring into a highly-stressed poly-axial (3D) flat-jack loaded cell of 50 x 50x 50cm size, in a direction deviated to one principal stress. (Addis et al., 1990). The three-dimensional nature of the fracturing, with fracturing also ahead of the face, has been experienced in some deep TBM tunnels. In the middle of Figure 2 (left) the world's first significant TBM tunnel is shown. This 2.2m diameter and nearly 1 km long tunnel was driven by a Beaumont TBM in 1880, using steam-power. The chalk marl of the adjacent Channel Tunnels, driven between the UK and France some 110 years later, has a uniaxial compressive strength σ_c of only 4 to 9MPa. The failure of the haunches in this pioneer pilot tunnel occurred where it passed under a 70m high cliff with a consequent approximate 2MPa increase of vertical stress. We can assume that the ratio of σ_θ/σ_c ratio would have exceeded 0.4 by a significant margin.

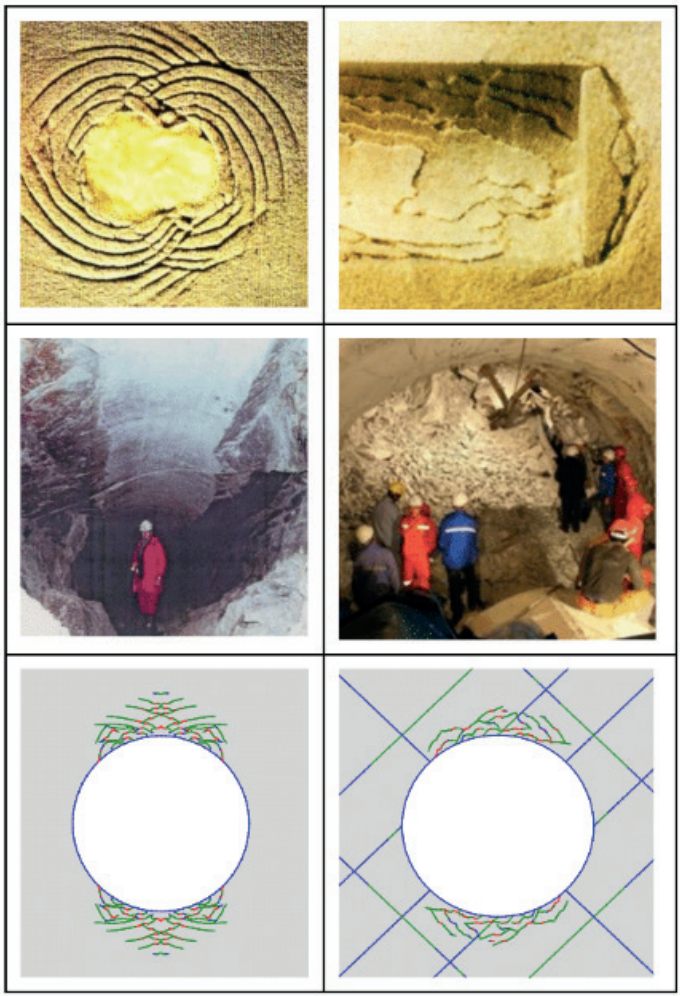

Figure 2. Examples of 'stress-induced', or more correctly extension-strain induced fracturing, followed by propagation-in-shear. (Top) sandstone tunnel models, (middle) two real TBM tunnels from 1880 and 2009 (chalk marl and marble). The two FRACOD models simulate deep TBM excavations: intact or jointed granite.

The TBM photograph showing complete tunnel collapse is the result of a tragic rock-burst accident in a very deep TBM pilot tunnel of 5m diameter in China. This was bored in insufficiently strong, originally massive marble with σ_c of 70-120MPa. The tunnel depth was typically 1 to 2.5 km. All tunnels in this big hydropower project (Jinping II) finally saw the TBM-driven headrace tunnels replaced by slightly less hazardous drill-and-blasting. In the latter, the highest tangential stresses are displaced a bit deeper into the surrounding rock due to the fracturing caused by the blasting.

FAILURE IN EXTENSION

Based on the extension-strain theory, which was promoted by Stacey, 1981, if the strain in a given direction becomes tensile and reaches a critical value, tensile fracturing will occur. A two-dimensional equation for expressing extension strain (in the lateral direction) is as follows:

$$\varepsilon_3 = [\sigma_3 - v\sigma_1] / E' \quad (1)$$

where v is the Poisson's ratio of the intact rock and E' is the generalised term for Young's modulus (E). (While E' = E for the plane stress condition; E' = E/(1-v^2) for plane strain, i.e. when no expansion in third dimension.

According to Equation (1), tensile strain may occur in a stress field where both principal stresses are compressive due to Poisson's effect. This explains why tensile fracturing can occur in the roof/wall of an underground opening, *and also behind a cliff or mountain wall*, where no tensile stress is expected. The only requirement will be that $v\sigma_1 > \sigma_3$, i.e. the disparity between the major principal stress (σ_1) and the minor principal stress (σ_3) needs to be high enough. This condition is met near to a tunnel wall, because the radial (= minor principal) stress becomes much lower than the tangential (= major principal) stress. Since Poisson's ratio is frequently about 0.25, a location where the stress ratio $\sigma_{1/} \sigma_3 > 4$ is required as an absolute minimum, but in fact sufficiently diverging principal stresses are required to generate significant lateral strain to cause tensile fracturing. The critical tensile strain for tensile fracturing to occur can be determined using the tensile strength of the rock. We can simply express this as:

$$\varepsilon_c = \sigma_t / E' \quad (2)$$

Using the critical tensile strain in Equation 2 to replace ε_3 in Equation 1 we obtain (by elimination of E' from both sides of the new equation), the critical compressive (i.e. tangential) stress for tensile fracturing (or spalling) to occur:

Since $\sigma_t/E' = [\sigma_3 - v\sigma_1] /E'$ therefore:

$$\sigma_1(\text{spalling}) = (\sigma_t + \sigma_3)/v \quad (3)$$

Considering that the confining stress σ_3 is zero at the wall of an underground opening (*and next to a cliff or mountain wall*) then for rocks with, typically UCS ≈ $10\sigma_t$ and Poisson's ratio ≈ 0.25, it means that tensile fracturing will start when the tangential stress reaches ≈ 0.4 σ_c. This in fact is the simple arithmetic source of the 'magic ratio' (0.4±0.1) that we saw

in Figure 1 following Martin et al. 1998, and confirming earlier observations of spalling and rock bursts in deep (or anisotropically stressed) Norwegian tunnels, as utilized by Grimstad and Barton, 1993 for quantifying SRF, the stress reduction factor, which is used to increase tunnel support via the rock mass classification Q-system.

NEW FORMULAE FOR VERTICAL CLIFFS

We will now leave the discussion of failure in deep tunnels, and concentrate on *cliffs and mountain walls*. We will also view evidence of extension strain fracturing in the form of planar sheet jointing from the world of rock climbing. Curved mountain slopes like the back of Yosemite's Half Dome in California are not the only reason for sheeting joint development. Figure 3 shows some compelling evidence for the range of 'cliff' heights apparently caused by the wide range of compression strength of rock. The world's highest almost vertical mountain walls top out on either side of 1,300m. The probable record is 1,340m for Great Trango Tower in the Karakoram, Pakistan. We may expect (laboratory-scale) compressive strengths of 100-150MPa for the granites in the highest walls, while in the case of Cappadocia's ancient cliff dwellings in porous tuff in Turkey, the strength may be only 1MPa, limiting cliff heights to the frequently observed 15-20m. The key to the huge range of heights illustrated in Figure 3 is that the *tensile strengths* of rocks may range from no more than 5-10MPa for exposed granite, down to 0.05-0.1MPa for exposed tuff. Numerous examples of the latter are given by Aydan and Ulusay, 2003. All tensile strengths tend to get downgraded by weathering during millennia of thermal cycles, which may exceed a 70-80°C annual range, and vary strongly even during one day. The big range of what are in fact 'limited' cliff and mountain-wall heights, can be roughly explained by comparing the assumed maximum vertical stress (the critical spalling stress in this case) with *extensional strength* σ_t/v. To do this involves comparing cliff height and rock density, with the ratio of tensile strength and Poisson's ratio.

$$H_{critical} = 100.\sigma_t/\gamma v \qquad (4)$$

(where σ_t is tensile strength in MPa, γ is density in tons/m^3, and v is Poisson's ratio).

Figure 3. The left-side photographs are examples of extreme mountain walls in hard or very hard rock. a) Great Trango Tower, Karakoram, Pakistan: approx. 1,350m, b) Mirror Wall, Baffin Island, Canada: approx. 1,200m, c) El Capitan granites, Yosemite: 950-1,000m. d) West Temple sandstones, Zion, Utah: 650-700m, e) Beachy Head bedded chalk, England: 75-100m, f) Cappadocia tuff, Turkey: 15 to 20m.

Note that the multiplier of 100 in equation 4 is purely a function of convenience when using typical rock mechanics strength units, expressed in MPa. With strength in kN/m^2 and density in kN/m^3 the '100' can be dispensed with. With equation 4 in mind, one should refer to the worked examples in Table 2, where realistic values are employed, for a wide spectrum of possible rock conditions, ranging from uniaxial compression strengths of 150MPa typical for hard granite, down to just 1.0MPa which might be typical for a weakened porous tuff, as found in the cliffs of Cappadocia, depicted at the bottom of Figure 3.

$\sigma_c = 150$MPa Very hard rock	$\sigma_c = 50$MPa Medium hard rock	$\sigma_c = 15$MPa Low strength rock	$\sigma_c = 1.0$MPa Very low strength rock
$\sigma_t \approx$ 9MPa	$\sigma_t \approx$ 3MPa	$\sigma_t \approx$ 1MPa	$\sigma_t \approx$ 0.05MPa
$\nu = 0.25$	$\nu = 0.20$	$\nu = 0.15$	$\nu = 0.15$
$\sigma_t / \nu = 36$MPa	$\sigma_t / \nu = 15$MPa	$\sigma_t / \nu = 6.7$MPa	$\sigma_t / \nu = 0.33$MPa
$\gamma = 2.8$ ton/m^3 $H_{crit} = 1{,}290$m	$\gamma = 2.5$ ton/m^3 $H_{crit} = 600$m	$\gamma = 2.25$ton/m^3 $H_{crit} = 296$m	$\gamma = 2.0$ ton/m^3 $H_{crit} = 16$m

Table 2. Examples of vertical height limits for near-vertical mountain walls and cliffs, over two orders of magnitude of rock strength, based on the application of equation 4.

In general, the ratio of compressive and tensile strengths for rock are in the range of $5 < \sigma_c/\sigma_t < 20$. However, in Table 2, since (compared to tunnels), cliffs and mountains are exposed to weathering forever, we made relatively conservative estimates of tensile strength σ_t. The proposed $\sigma_t/\gamma\nu$ mechanism of extension failure has the effect of steepening and degrading mountain faces. The sketches and photographs presented in Figure 4 show several aspects of the extensional mechanism. Because tensile strength is slowly reduced nearest to an exposed cliff or mountain face by constant cycling of temperature and moisture, it becomes easier for slabbing to occur. With assumed microcracking and grain-scale ice pressures, one may surmise an effective increase in Poisson's ratio, together with reduced near-surface tensile strength. If broadly correct, extension failure due to the σ_t/ν 'mechanism' would become easier with time. This is probably the true cause of the relative frequency of slabbing due to the 'constant' propagation of sheet jointing. We will return to this subject later.

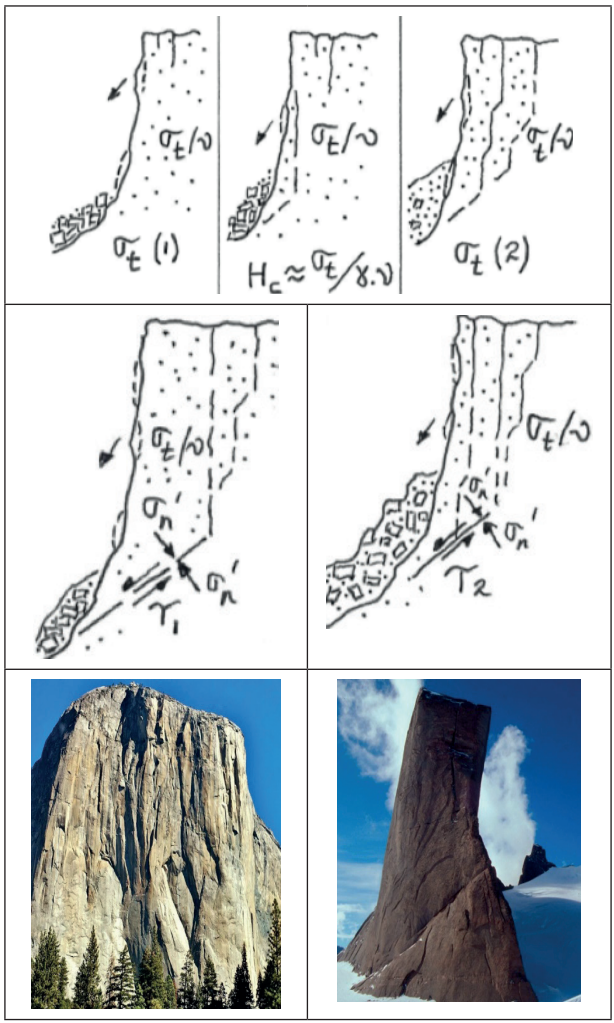

Figure 4. Top: Sketches illustrating the extensional strain failure mechanism involving the overcoming of the extensional strength σ_t /v. Also shown is the possibility of rock avalanche-scale basal shear failures, due to adverse tectonic structures. This is slightly developed at El Capitan in Yosemite, 1,000m in height (bottom-left), but apparently well developed at Holtanna, a 750m high monolith, in Dronning Maud's Land, Antarctica (bottom-right). (Here there may be an unintended but probable camera rotation of 5° - the Holtanna 'potential failure plane' should probably be approximately 5° steeper.)

The estimation of basal shear strength could be based on a combination of the strength components shown in Figure 5, since a final 'cascading' of failure may be involved (i.e. not linear Mohr-Coulomb or non-linear Hoek-Brown 'c + σ_n tan ϕ', but more correctly 'c then σ_n tan ϕ', as increasingly emphasized in some recent literature). Most likely: failure of remaining intact 'bridges', then shearing (or not) on these new, fresh, rough surfaces, then mobilization (or not) along the already established shear plane (or prior tectonic structure), and finally the limited strength of any clay-filled discontinuities or faults, displaying the lowest shear stiffness. (Barton, 2013).

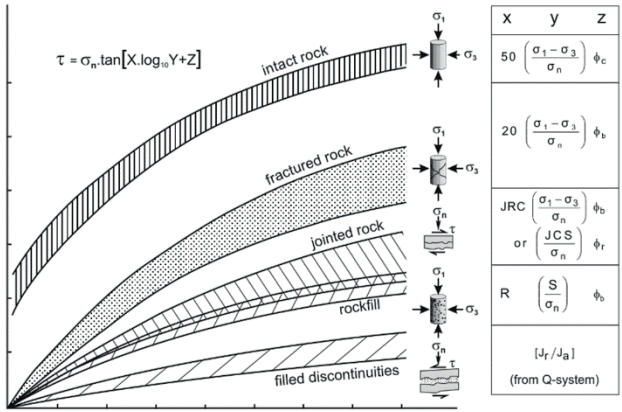

Figure 5. Representation of shear strength components in the form of laboratory tests, from *Barton*, 1999. Several components of strength may be involved when a large-scale body of rock is approaching failure. These linear approximations are often misleading when a significant range of stress is involved, as emphasized by Barton, 2013, 2016.

Although rock-surface curvature obviously helps for generating tensile stress as suggested by Martel, 2017, it is not a necessary condition for generating sheeting joints. The classic curved sheeting joints on 'the back' of Yosemite's Half Dome have alternative means of development than the curvature, and indeed are remarkably planar up the 750m vertical face. The planarity needs an explanation because sheeting joints are often completely planar over long distances, bot horizontally and vertically, as can be vouched for by rock climbers, and as can be seen in thousands of rock-climbing photographs. Interesting sources here are the following: Davis, 2013, Honnold and Roberts, 2016 and Florine and Moye, 2016. For the case of the Cappadocia tuffs, careful studies by Aydan and Ulusay, 2003 and many others, have shown that temperature (freeze-thaw) cycling and moisture-content cycling have a degrading effect on compression and tensile strength. There is an effective annual temperature range of 70 to 80° C even in the shade, and this may even be increased for cliffs in direct sunlight. In the Alps, specifically the Matterhorn, the gradual degradation of the highest rock which is in almost permafrost conditions, has been nicely described by Weber et al., 2016.

SOIL MECHANICS FORMULATIONS ARE NOT APPROPRIATE FOR FAILURE OF INTACT BRITTLE ROCK

Concerning the question of limiting cliff and mountain wall heights it is appropriate to present and then check classic soil mechanics based solutions which at their simplest, involve a linear shear strength envelope defined by cohesion and friction (c and ϕ). The Coulomb shear strength assumption, with allowance for Terzaghi's law of effective stress, assuming water pressure (u) along the failure plane, is as follows:

$$\tau = c + (\sigma_n - u) \tan \phi \quad (5)$$

Assuming a planar shear failure surface, dipping from the ground surface down to the toe of an imaginary vertical cliff, *lowerbound* and *upperbound* solutions can be obtained, based on limit equilibrium or limit theory analysis. Soils mechanics texts such as Verruijt, 2001 indicate the following range of solutions for critical heights of vertical cuts in soils i.e.Fig. 6.

$$2c/\gamma \tan(45°+\phi/2) \leq H_c \leq 4c/\gamma \tan(45°+\phi/2) \quad (6)$$

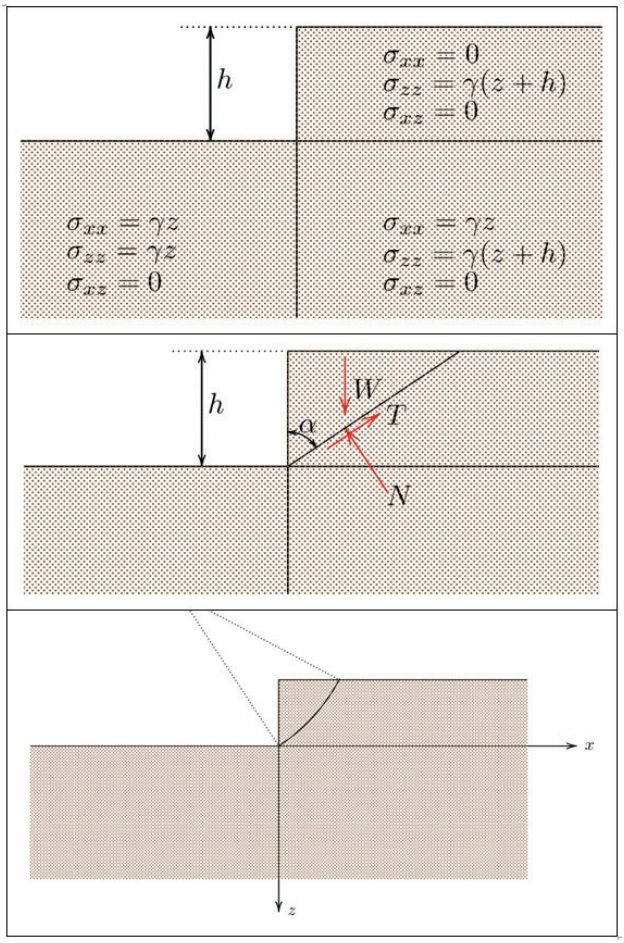

Figure 6. Several approaches to the stability of a vertical cut appear in soil mechanics literature. The top example (a) shows the assumed equilibrium of three zones and gives a *lowerbound* solution. The bottom example (b) illustrates an *upperbound* solution involving a specific shear surface. After Verruijt (2001). The circular failure surface assumption was used by Fellenius, 1927.

Equation 6 gives a surprisingly large (2:1) range. Furthermore, because soil fails differently to intact rock, we find that the estimates of H_c if (erroneously) used for rock cliffs or mountain walls are, remarkably, from 3 to 6 times in error, as indicated in the worked examples below. Note that a circular failure surface gives 3.85 for the multiplier. An exact solution is elusive according to Verruijt, 2001, and matters do not get easier if non-linear shear strength is considered. The lower bound of equation 6 is usually attributed to Drucker and Prager, 1952 and is referred to as the static solution, in contrast to the 'dynamic' solution with multiplier '4'.

Concerning the trial evaluation of 'soil mechanics' formulations summarized in equation 6, we need to make appropriate estimates of cohesion. A lowerbound estimate of cohesion (c) for rock would be obtained most simply by assuming a straight-line, rather than a curved tangent between the uniaxial tension (σ_t) and uniaxial compression (σ_c) Mohr circles. The simple equation for the lowerbound cohesion intercept (c), derived from Mohr circle geometry, was given in Barton, 1976:

$$c = \tfrac{1}{2} (\boldsymbol{\sigma}_c.\boldsymbol{\sigma}_t)^{1/2} \qquad (7)$$

We can examine the foregoing formulations with examples of a moderately strong valley-wall sandstone (UCS = 75 MPa) and a massive-scale mountain-wall in granite (with UCS = 150MPa). We will assume that $\boldsymbol{\sigma}_c/\boldsymbol{\sigma}_t \approx 15$. (The expected laboratory-test range of $\boldsymbol{\sigma}_c/\boldsymbol{\sigma}_t$ could range from 5 to 20: but 8 to 16 is more likely). The following strength assumptions are used:

1. Sandstone $\boldsymbol{\sigma}_c$ = 75MPa, $\boldsymbol{\sigma}_t$ = 5MPa c = ½(75x5) $^{1/2}$ = 9.7MPa
2. Granite $\boldsymbol{\sigma}_c$ = 150MPa, $\boldsymbol{\sigma}_t$ = 10MPa c = ½(150x10) $^{1/2}$ = 19.4MPa

The gradient (ϕ = internal friction angle) of the presently assumed straight line between the tensile and compressive strength Mohr circles, giving a *lowerbound* value of c is as follows:

$$\boldsymbol{\sigma}_c/\boldsymbol{\sigma}_t = \tan^2(45° + \phi/2) \qquad (8)$$

A friction angle ϕ of approximately 61° is indicated if σ_c/σ_t =15, as assumed. Using just the *lowerbound* soil mechanics solution given by equation 6, serious errors of mountain wall heights are evident. Note the following density assumptions: 25kN/m^3 for sandstone, 27.5kN/m^3 for granite.

Sandstone 'valley wall' $H_c = 2c/\gamma \tan(45° + \phi/2)$ H_c=2x9.7x1000/25 tan (45° + 30.5°) = 3,001m

Granite 'mountain-wall' H_c=2x19.4x1000/27.5 tan (45°+ 30.5°) = 5,456m

By comparison equation 4 (specifically applying to brittle rock) suggests H_c limits of:

Sandstone: $100.\sigma_t/\gamma v = 100.5/2.5 \times 0.25 = 800m$

Granite: $100.\sigma_t/\gamma v = 100.10/2.75 \times 0.25 = 1{,}456m$

We may note from these solutions for rock, using the new formulation involving *extensional theory* (equation 4) that the real cases depicted in Figure 3 are informing us that it is not realistic to reckon with 'laboratory scale' (i.e. unweathered, optimal samples) tensile strengths. These two mountain-wall estimates of 800 and 1,456m are perhaps 20-30% too high, but much better than 300 or 600% too high if erroneously trying to apply soil mechanics methods (equation 6). Note again the more sensible *range* of height limits given in Table 2.

PLANAR SHEETING JOINTS FROM EXTENSION STRAIN MECHANISMS

To conclude this section about a new method of estimating cliff and mountain-wall heights, we can tentatively apply the σ_t /v method to explain the origin of sheet jointing. Our seemingly almost fearless free-solo rock climbers, who are constantly climbing these planes, and finger-wedging up the related sub-vertical crack systems. Statistics from well-documented climbing routes in the Yosemite Valley given by Stock et al. 2012 indicate that 'slabbing' or the fall of loosened sheeting joints is quite frequent. Indeed, there are frequent reports of changed climbing routes due to their occurrence, perhaps as frequently as every decade.

Figure 7 is a good demonstration of the extreme *planarity and smoothness* that can be a common characteristic of sheet-jointing or exfoliation, in this case in Zion sandstone and the vertical (front) wall of Yosemite's (Half Dome) granite. A curved surface, facilitating the tensile component, is not in fact a necessary condition for the development of sheet jointing, as argued in a comprehensive (two centuries) review by Martel, 2017. Note that the long sub-vertical cracks loved and indeed needed by rock climbers, are probably a large-scale expression of *extensional fracturing* in the perpendicular direction. An excellent example is shown in Figure 8, with Alex Honnold again free-soloing.

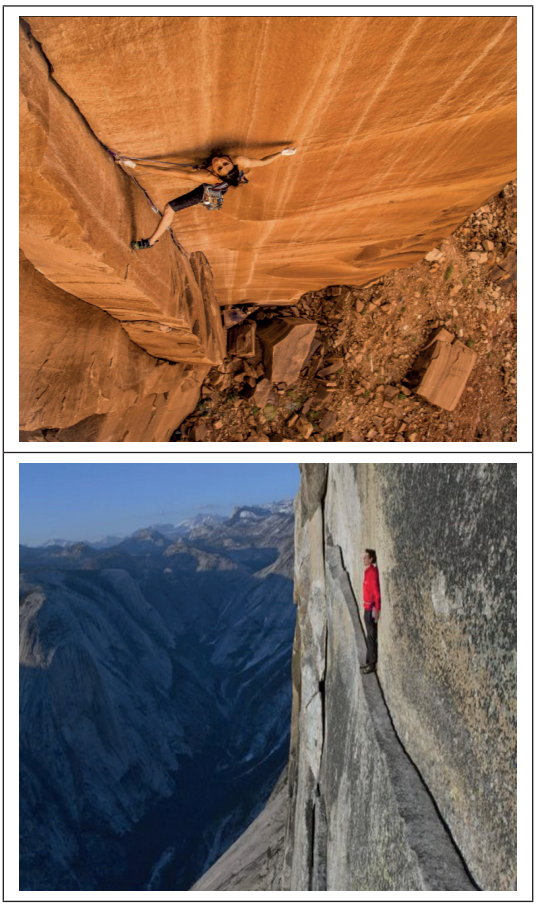

Figure 7. Two famous free-solo rock climbers: Steph Davis and Alex Honnold on sheeting joints in Zion national park and in Yosemite national park ('Thank God Ledge, Half-Dome) where Honnold made the first ever free-solo ascent. Refer to Davis, 2013, and Honnold and Roberts, 2016 for some remarkable examples of planar sheeting joints. Rock and mountain climbing, as shown in countless internet sites, is a particularly rich source of examples of rock exposures at all scales, for those interested in rock fracture mechanics principles.

MAXIMUM SLOPE ANGLES WHEN ROCK MASSES ARE JOINTED

This paper has so far treated rock masses as if they were intact or sparsely jointed, both in the case of the fracturing in deep tunnels, and in the case of the limiting heights of cliffs in weaker rock, and mountain walls in strong rock. If instead, *jointing is present*, it has been assumed not to significantly alter the extension strain fracturing mechanism. However, is doubtful that this assumption is generally valid, but it may be acceptable in the case of cliff failures in (horizontally) bedded rock, since the tensile failure planes would be at right-angles to such beds. See for instance the cliff-front failures in chalk, Figure 3e.

Figure 8. Free-solo climber Alex Honnold on El Capitan. Extension fractures in the third dimension are the assumed origin. Such features may be hundreds of meters in extent and seem to be formed by mountain-induced stress (and strain) rather than being a part of a pre-existing major joint pattern.

Methods have recently been developed for selecting safe and maintenance-free rock slope angles in *more general jointed conditions.* The method is called Q_{slope}, with general similarity to the Q-system for tunnels. In fact the first four parameters are unchanged, except for the use of oriented Jr/Ja ratios to allow for wedges formed with two joint sets having different Jr/Ja magnitudes, and therefore potentially different influences on instability. The method was introduced by Barton and Bar, 2015 and more recently described by Bar and Barton, 2017 after the collection of more than 400 case records, mostly by co-author Neil Bar.

$$Q_{slope} = \frac{RQD}{J_n} x \left(\frac{J_r}{J_a} \right)_0 x \frac{J_{wice}}{SRF_{slope}} \qquad (9)$$

As with the Q-system, the rock mass quality in Q-slope can be considered a function of three parameters, which are crude measures of:

1. Block size: (RQD/J_n).
2. Shear strength: (J_r/J_a) or average shear strength in the case of wedges $(J_r/J_a)_1 \; x \; (J_r/J_a)_2$.
3. External factors and stress: (J_{wice}/SRF_{slope}).

Barton and Bar, 2015 derived a simple formula for the steepest slope angle (β) not requiring reinforcement or support for slope heights less than 30m. This formula has now been extended to much larger slope heights:

$$\beta = 20 \log_{10} Q_{slope} + 65° \quad (10)$$

Equation 9 matches the central data for stable slope angles greater than 35° and less than 85°. From the Q-slope data, the following correlations are simple and easy to remember:

- Q-slope = 10 - slope angle 85°
- Q-slope = 1 - slope angle 65°
- Q-slope = 0.1 - slope angle 45°
- Q-slope = 0.01 - slope angle 25°

Numerous case records are illustrated in Figure 9. The following example from Bar and Barton, 2017 gives some insight into this simple method, and Figure 10 illustrates the concept for the case of open pit bench angles, obviously in jointed, as opposed to sparsely jointed rock.

A 30m high slope was excavated at an angle of 65° and failed shortly after. The wedge failure occurred in weak, moderately weathered sandstone (σ_c = 35MPa). The following Q-slope ratings were assigned during the back-analysis:

RQD = 40-50%

J_n = 9

Set A: J_r = 1, J_a = 4, O-factor = 0.5

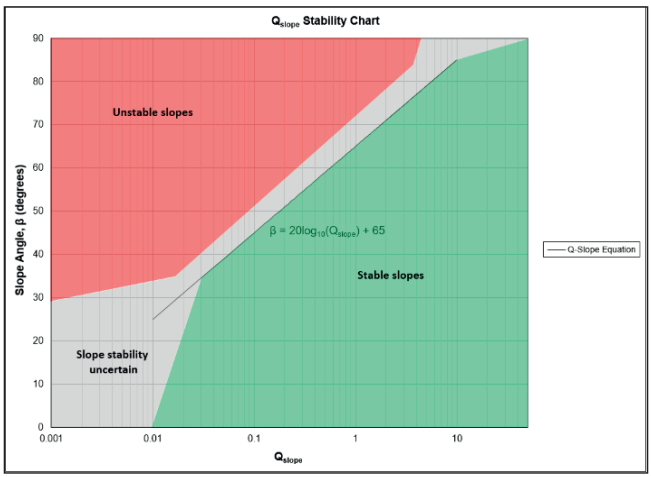

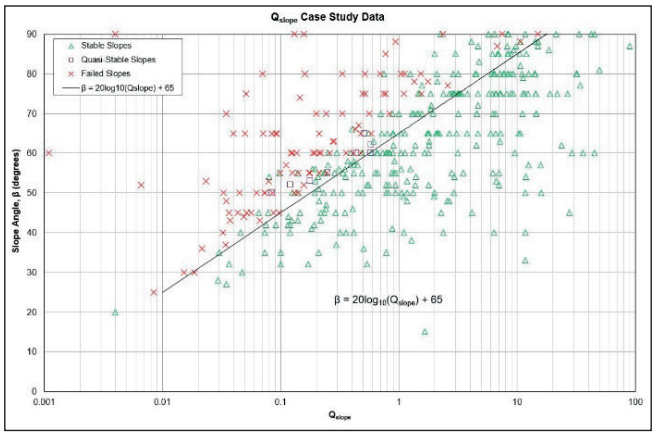

Figure 9. The coloured areas indicate stable (green) and unstable (red). The case records show fairly consistent separation, with a transition zone (grey). Bar and Barton, 2017.

Set B: $J_r = 3$, $J_a = 4$, O-factor = 0.9

Set C: Release plane or tension crack that did not contribute to the overall shear strength of the wedge.

$J_{wice} = 1$ (desert environment, competent rock and generally stable structure where Set B has limited continuity).

$SRF_a = 2.5$ (slight loosening due to surface location), $SRF_b = 2.5$, SRF_c = N/A.

Based on the assigned ratings, Q-slope and β were estimated as follows:

$$Q_{slope} = \frac{55}{9} x \left[\left(\frac{1}{4} x 0.5 \right) \left(\frac{3}{4} x 0.9 \right) \right] x \frac{1}{2.5} = 0.206$$

$$\beta = 20 \log_{10}(0.206) + 65° = 51°$$

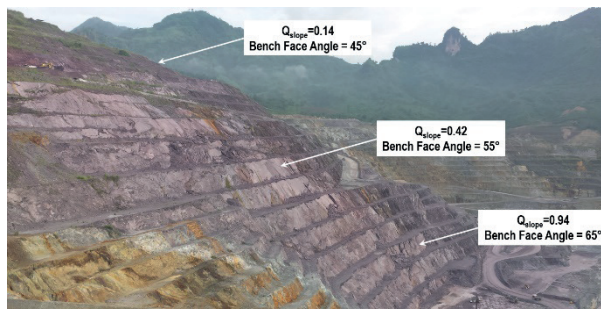

Figure 10. An open-cast slope in Laos, showing increasing values of Q_{slope} and slope angles, as greater depth and sounder rock is reached. Bar and Barton, 2017.

Q-slope suggested an angle of 51° would have resulted in a stable slope (i.e. approximately 15° shallower than excavated and consistent with kinematic analysis).

MOUNTAIN HEIGHTS LIMIT OF 8 TO 9KM

Increasing the scale dramatically, one can tentatively suggest that the highest mountains of 8,000 and 9,000m are not due to the 'limited' uniaxial compression strength as sometimes proposed, but are due to critical state, non-linear rock mechanics. The limiting strength is more likely to be given by the top (horizontal) part of a rock's strongly curved shear strength envelope, or perhaps by the slightly lower brittle-ductile transition. Figure 11 in fact demonstrates similar magnitude for the critical confining pressure and the magnitude of uniaxial compressive strength, such as 200 MPa, as shown by Singh et al. 2011.

Note that the overall curvature of the suggested shear strength envelope (Figure 11) is somewhat greater than that of Hoek-Brown, which is presently one of the most used non-linear strength envelopes for intact rock.

The world's highest mountains (14 peaks of 8,000 to almost 9,000m height, with Everest at 8,848m: Figure 12) cannot be limited by the uniaxial compression strength of rock. This is because the rock strength would need to be the *confined compression strength* (σ_1 in Figure 11), since great depth is obviously involved where stress and strength are (almost) in equilibrium. The possible range of perhaps 600 to 900MPa for the confined compressive strength of strong igneous or metamorphic rocks at 10km depth would support mountains of 20 to 30 km height.

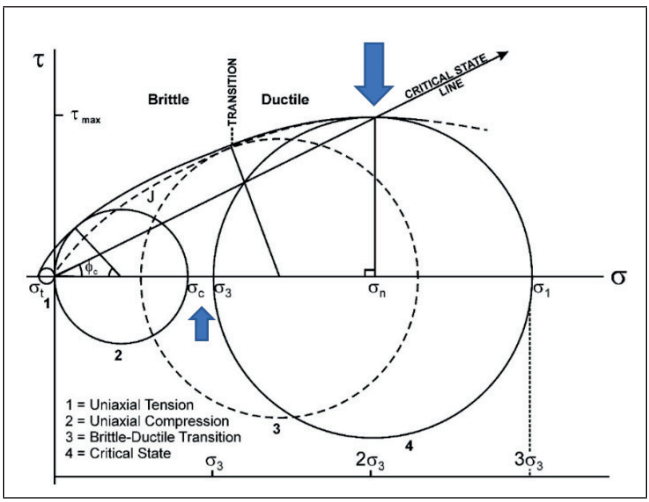

Figure 11. The curved failure envelope for intact rock up to the critical state proposed by *Barton*, 1976. The critical state marks the location of the maximum possible shear strength for a given rock type. The uniaxial tensile (1) and uniaxial compression (2) Mohr circles are shown on the left, and provide the lower-bound estimate of cohesion c, that was utilized earlier. Singh et al. 2011, in a major review, have shown that the critical confining pressure is equal or close to, the uniaxial compression strength (see small blue arrow). Both the deviation from linear Mohr-Coulomb, and the equation of the curved envelope are developed (by Singh et al. 2011, and by Shen et al. 2018).

The empirical evidence of millions of years is therefore violated if trying to use the (confined) compression strength of the rock, and rock mechanics principles are actually violated by those suggesting use of the 200-300 MPa if referring to the use of *uniaxial strength*. The fourteen mountains in the exclusive 8 to 9 km height class provide empirical evidence of total vertical stresses that might be as high as 9,000 x 3/100MPa = 270MPa, assuming a composite density as high as 3.0. If there could be a pore/joint water pressure as high as 50MPa (with some upper drainage into valleys assumed here), then tentative application of the law of effective stress brings us to a principal effective vertical stress of 220MPa. This would apply in the lower part of a potential shear failure surface. However, we need to consider the shear stress generated by this effective vertical stress of 220MPa. On a nominal plane inclined at 45° this could be as low as 150MPa, considering round figures. In case of an elevated horizontal stress (i.e. $k_0 > 1$), equilibrium would be improved, and a higher mountain could be supported before reaching a shear strength limit.

Figure 12. Mount Everest at 8,848m (extract from Wikipedia photo). It is proposed that it's maximum height is shear-strength limited, following a critical state rock mechanics limit, as shown in Figure 8.

CONCLUSIONS

Tensile strength and Poisson's ratio explain the limited maximum heights of cliffs and steep mountain walls, and the origin of planar sheeting joints. A range of maximum heights from 20m in tuff, 100m in chalk, 650m in sandstone, to 1,300m in granite can be sensibly quantified by considering failure caused by extensional strain and fracturing in tension in each case. There are parallels in the world of deep tunnels in hard rock. The widely quoted critical tangential stress of 0.4 x UCS that may be reached by deep hard-rock tunneling should be replaced by the ratio σ_t/v, i.e. initial tensile failure which is mobilized by extensional strain. These two ratios are numerically equivalent. Shear strength and tensile strength, ably assisted by Poisson's ratio, are inevitably the weakest links in 'high-stress' structural geology and in the more typically 'low-stress' processes in geomorphology, respectively. When rock masses are jointed the extension strain-induced failure mechanism may no longer apply, and stability has to be assessed by characterizing the properties of

the jointing. The Q_{slope} method is proving to be useful here. The highest mountains of 8,000-9,000m are limited by maximum shear strength, not by compressive strength. The confined strength of competent mountain-forming rock is several times too high.

REFERENCES

Addis, M.A., Barton, N., Bandis, S.C. & Henry, J.P. (1990). Laboratory studies on the stability of vertical and deviated boreholes. 65th Annual Tech. Conf. and Exhib. of Soc. of Petroleum Engineers, New Orleans.

Aydan, Ö. And R. Ulusay, (2003). Geotechnical and geoenvironmental characteristics of man-made underground structures in Cappadocia, Turkey. Engineering Geology, 69, 245-272.

Bar, N. and N. Barton, 2017. The Q-slope method for rock slope engineering. Rock Mechanics and Rock Engineering. Springer.

Barton, N. (1976). The shear strength of rock and rock joints. Int. Jour. Rock Mech. Min. Sci. and Geomech. Abstr., Vol. 13, No. 9: 255-279.

Barton, N. 1999. General report concerning some 20th Century lessons and 21st Century challenges in applied rock mechanics, safety and control of the environment. Proc. of 9th ISRM Congress, Paris, 3: 1659-1679, Balkema, Netherlands.

Barton, N. & Infanti, N. (2004). Unexpected stress problems in shallow basalts at the Ita hydroelectric power project in S.E. Brazil. Proc. ARMS 2004 : 3rd Asian Rock Mechanics Symposium, Kyoto.

Barton, N. (2013). Shear strength criteria for rock, rock joints, rockfill and rock masses: problems and some solutions. J. of Rock Mech. & Geotech. Engr., Elsevier 5(2013) 249-261.

Barton, N. and Grimstad, E. (2014). Q-system - an illustrated guide following forty years in tunnelling. 43 p. Web site www.nickbarton.com.

Barton, N. and N. Bar, 2015. Introducing the Q-slope method and its intended use within civil and mining engineering projects. EUROCK 2015 & 64th Geo-mechanics, Salzburg.

Barton, N.R. (2016). Non-linear shear strength descriptions are still needed in petroleum geomechanics, despite 50 years of linearity. 50th US Rock Mech. Symp. ARMA 16, 252, 12 p.

Barton, N. and Shen, B. (2017). Risk of shear failure and extensional failure around over-stressed excavations in brittle rock. J. of Rock Mech. & Geotech. Eng., Vol.9, No.2, 210-225. Elsevier.

Davis, S. (2013). *Learning to Fly: An Uncommon Memoir of Human Flight, Unexpected Love, and One Amazing Dog.* A Touchstone Book, Simon & Schuster, New York, 292p.

Drucker, D. C. and Prager, W. (1952). Soil mechanics and plastic analysis or limit design, Quarterly of Applied Mathematics, 10, 157-165.

Florine, H. and J. Moye, (2016). *On the Nose – A lifelong obsession with Yosemite's most iconic climb.* Rowman & Littlefield/ Falcon & National Book Network. 203p.

Grimstad, E. & Barton, N. (1993). Updating of the Q-System for NMT. Proc. of Int. Symp. on Sprayed Concrete – Modern Use of Wet Mix Sprayed Concrete for Underground Support, Fagernes, 1993, Eds Kompen, Opsahl and Berg. Norwegian Concrete Association, Oslo, 46-66.

Honnold, A. and D. Roberts, (2016). *Alone on the Wall.* W.W. Norton & Company, New York. 248p.

Martel, S.J. (2017). Progress in understanding sheeting joints over the past two centuries. Jour. of Structural Geology, Elsevier, 94, 68-86.

Martin, C.D., Kaiser, P.K. & McCreath, D.R. (1998). Hoek–Brown parameters for predicting the depth of brittle failure around tunnels. Can. Geotech. J. 36, 136-151.

Shen, B., Stephansson, O. & Rinne, M., (2013). *Modelling Rock Fracturing Processes: A Fracture Mechanics Approach Using FRACOD.* Springer, 173p.

Shen, B. and N. Barton (2018). Rock fracturing mechanisms around underground openings. Geotechnical Engineering Journal, Korea (in press).

Shen, B., Shi, J. & N. Barton, (2018). An Approximate Non-Linear Modified Mohr-Coulomb Shear Strength Criterion with Critical State for Intact Rocks. Journal of Rock Mech. and Geotech. Eng. (in press).

Singh, M., Raj, A. and B. Singh. (2011). Modified Mohr-Coulomb criterion for non-linear triaxial and polyaxial strength of intact rocks. Int. J. Rock Mech. Min. Sci., 48(4), 546-555.

Stock, G.M., N. Luco, B.D. Collins, E.L. Harp, P. Reichenbach, and K.L. Frankel, (2012). Quantitative rock-fall hazard and risk assessment for Yosemite Valley, Yosemite National Park, California. USGS.

Stacey, T.R. (1981). A simple Extension Strain Criterion for Fracture of Brittle Rock. Int. J. Rock Mech. Min. Sci. & Geomech. Abstr. 18, 469-474.

Terzaghi, K. (1962). Stability of steep slopes on hard unweathered rock. Geotechnique 12:251-263.
Verruijt, A. (2001). Soil Mechanics. Delft University of Technology, The Netherlands.

Weber, S., J. Beutel, J. Faillettaz, A. Hasler, M. Krautblatter and A. Vieli. (2016). Quantifying irreversible movement in steep fractured bedrock permafrost at Matterhorn (CH). The Cryosphere Discussions Journal.